

# Electrochemical Machining of Nickel-based Cast Casing using a Cylindrical Rotating Electrode

Yongcheng Ge<sup>1,2,\*</sup>, Zengwei Zhu<sup>2</sup> and Yongwei Zhu<sup>1</sup>

<sup>1</sup> College of Mechanical Engineering, Yangzhou University, Yangzhou, China;

<sup>2</sup> College of Mechanical and Electrical Engineering, Nanjing University of Aeronautics and Astronautics, Nanjing, China; zhuzw@nuaa.edu.cn (Z. Z.); ywzhu@yzu.edu.cn (Y. Z.)

\*E-mail: [zhge@yzu.edu.cn](mailto:zhge@yzu.edu.cn)

Received: 5 April 2019 / Accepted: 8 June 2019 / Published: 31 July 2019

---

Nickel-based superalloys are a diverse group of materials commonly used for components such as aero engine blades, guides and the cartridge receiver in the hot sections of gas and steam turbines. To satisfy the high-precision manufacturing requirements for engine components, the casting components often need to be processed to remove residual material formed in the casting process. However, with traditional processing methods, the material properties of nickel-based alloys such as high strength at elevated temperatures, high work hardening, and low thermal diffusivity invariably translate into poor machining characteristics. In this study, electrochemical machining (ECM) is employed to remove the casting allowance for a particular design of a simulated cartridge receiver. Two processing methods, designed to achieve a high machining efficiency, were evaluated and the basis for selection of the methods is discussed. Theoretical analysis and simulation results show that a single feed method was more suitable than a cyclic feed method for removal of the casting allowance. Further, it was experimentally demonstrated that the machining accuracy of the single feed method is better than that of the cyclic feed method, and the processing efficiency was also improved significantly for the former.

---

**Keywords:** Nickel-based superalloys; electrochemical machining; cylindrical electrode; tool trajectory

## 1. INTRODUCTION

Cast nickel-based superalloys are an important class of advanced alloy typically used in high-temperature applications, in which high strength, excellent corrosion resistance, and good fatigue resistance are required [1,2]. A major application of these alloys is in the hot section of gas and steam turbine components, such as aero engine blades, guides, and cartridge receivers [3,4]. To satisfy the high-precision manufacturing requirements for engine components, the casting components often need to be processed to remove the residual material formed in the casting process, such as the cast allowance and the casting riser materials. However, given the properties of nickel-based alloys such as high strength

at elevated temperatures, high work hardening, and low thermal diffusivity, there is generally poor machinability for traditional processing [5,6]. Therefore, it is necessary to develop alternative manufacturing technologies for machining such alloys.

The electrochemical machining (ECM) process is an anodic electrochemical dissolution process that efficiently removes materials with high accuracy and without limitations to the mechanical properties of the alloys [7,8]. Compared with traditional technologies, ECM does not produce heat-affected zones and internal stresses on the machining surface, nor does it cause tool wear. Therefore, ECM is becoming increasingly important for the production of sophisticated components using hard-to-machine materials [9,10].

In recent years, many researchers have focused on the machining of hard-to-machine materials using ECM. Klocke et al. conducted basic research on the electrochemical machinability of selected modern titanium and nickel alloys for aero-engine components [11]. Xu and Chen used an experimental approach to determine the optimal electrolyte composition and machining parameters for the ECM of Ti40 and Ti60, with the aim of producing blisk [12,13]. Weber et al. discussed the electrochemical dissolution characteristics of cast iron in a  $\text{NaNO}_3$  electrolyte, the studies focusing on the influence of the matrix composition, the graphite particle shape and the electrolyte pH [14]. Mimura et al. studied the electrochemical corrosion behavior of titanium castings and found that sandblasted surfaces showed a reduced passive region and a considerable increase in the passive current density [15].

Although, numerous ECM methods for different difficult-to-cut materials have been reported, there have been few investigations on the ECM of cast superalloys [16]. In this study, ECM is used to process a simulated sample of a particular design of cartridge receiver made from nickel-based superalloy K423A by an investment casting process [5,17]. To achieve high machining efficiency, two processing methods, a single feed and a cyclic feed method, were investigated, and the basis for method selection is described. Simulations were performed to aid in selection. The results showed that the single feed method achieved better machining efficiency than the cyclic feed method for removal of the cast allowance of the simulated sample. Experiments were also undertaken, and the results showed that the machining accuracy for the single feed method was better than that of the cyclic feed method, and the processing efficiency was significantly improved in the case of the former.

## 2. PRINCIPLES AND ANALYSIS

A schematic of the high-speed removal of the cast allowance by ECM is illustrated in Figure 1. A small-diameter cylinder with an inner flow passage is used as the cathode tool, with the aim of processing different forms of casting riser and machining allowances as part of a universal tool. In the ECM process, the cathode maintains a high rotation speed to ensure a uniform electric field and smooth removal of the electrolytic products. Simultaneously, the cathode tool can be fed perpendicular to the anode workpiece surface along the x-axis. The anode workpiece rotates around its axis, and the speed may be adjusted freely. The electrolyte is pumped into the cathode tool and transported directly to the machining area through the inner flow passage. When a voltage is applied, the machining allowances of the anode workpiece are removed gradually.

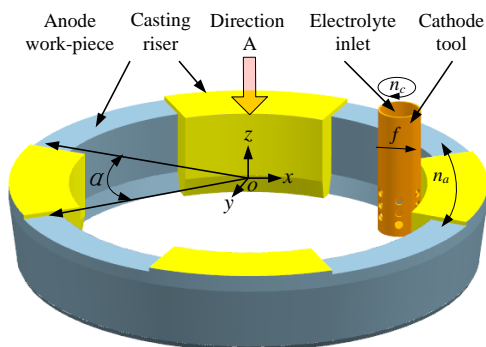


**Figure 1.** A schematic for high-speed ECM of the cast allowance.

To achieve high machining efficiency, two processing methods are proposed as shown in Figure 2. In Figure 2a, a single feed processing method is depicted, whereby the machining allowance is removed by a single feed through horizontal movement of the cathode perpendicular to the anode surface along the x-axis. Subsequently, the anode rotates slowly around its axis for feed motion. Figure 2b showed the cyclic feed processing method, in which the feed motion is achieved by the horizontal movement of the cathode perpendicular to the anode surface along the x-axis. In this process, the anode workpiece oscillates within a specified range.

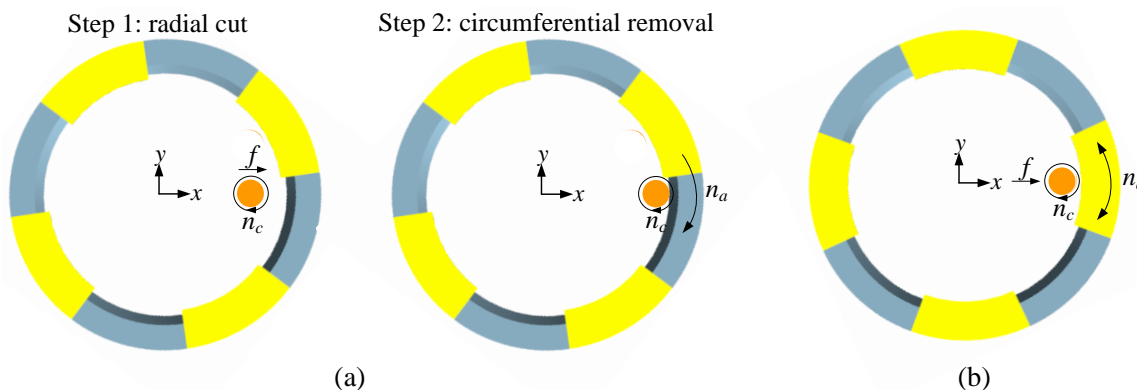


**Figure 2.** Schematic of the processing methods in the A-direction view: (a) single feed, (b) cyclic feed.

The tool paths for the two proposed methods are illustrated in Figure 3. As shown in Figure 3a, the anode speed should be precisely controlled because it acts as a feed motion. According to Faraday's law, the anode speed can be calculated as:

$$n_a = \frac{\eta \omega i}{2\pi r} \tag{1}$$

where  $\eta$  is the current efficiency,  $\omega$  is the volume electrochemical equivalent,  $i$  is the current density, and  $r$  is the anode radius after processing.

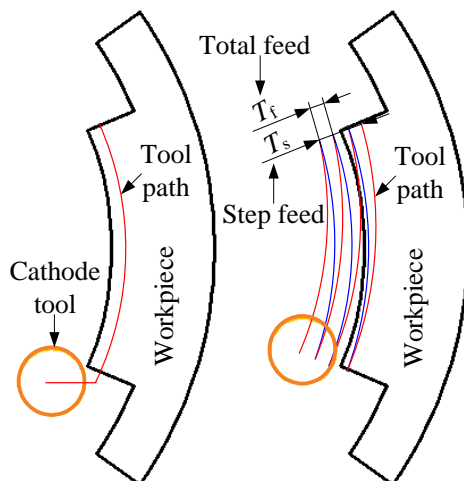


**Figure 3.** Tool path: (a) single feed, (b) cyclic feed.

For the cyclic feed method, the effect of the anode oscillation frequency (corresponding to the anode speed in the single feed method) can be expressed by the following equations:

$$T = n \cdot \frac{1}{n_a} \tag{2}$$

$$T = \frac{T_f}{f} \tag{3}$$

$$T_s = \frac{T_f}{n} \tag{4}$$

where  $T$  is the total processing time,  $n_a$  is the oscillation frequency of the anode workpiece,  $n$  is the number of anodic oscillations during the total processing time,  $T_s$  is the cathode feed in an oscillating period of the anode workpiece (Also known as the step feed rate),  $T_f$  is the total feed of the cathode, and  $f$  is the cathode feed rate.

Combining Eq. 1-3, the step feed rate can be expressed as follows:

$$T_s = \frac{f}{n_a} \tag{5}$$

Assuming that the cathode feed rate is constant, the higher the anode oscillation frequency, the smaller the step feed rate, i.e., the material removal uniformity is improved when the anode frequency is increased. Therefore, the fastest anodic oscillation frequency should be preferred in the cyclic feed method.

To compare the removal capability of the two processing methods,  $P$  may be used to express the ratio of the removal mass of the two methods:

$$P = \frac{M_s}{M_c} \tag{6}$$

where  $M_s$  and  $M_c$  represent the removal masses for single feed and cyclic feed, respectively.

According to Faraday's law, Eq. 6 can be expressed as follows:

$$P = \frac{t \cdot \eta k \int i_s d_l}{t \cdot \eta k \int i_c d_l} = \frac{\int i_s d_l}{\int i_c d_l} \tag{7}$$

where  $k$  is the mass electrochemical equivalent,  $i_s$  and  $i_c$  represent the current density for single feed and cyclic feed, respectively,  $t$  is the processing time and  $d_l$  is the arc element. Therefore, assuming that the processing parameters are consistent, the appropriate processing method can be chosen by determining the magnitude of  $P$ : For  $P < 1$ , the cyclic feed method should be preferred; for  $P = 1$ , the two methods should be equivalent. For  $P > 1$ , the single feed method should be preferred.

With some assumptions [18], analysis of the physical model may be simplified, as shown in Figure 4. Assuming that the ECM process is in a stable state, the applied voltage and the minimum inter-electrode gap were both set to 20 V and 0.25 mm, respectively. On the basis of the parameters described above, a simulation of the two methods was performed to obtain the magnitudes of the current densities via COMSOL software version 5.1.

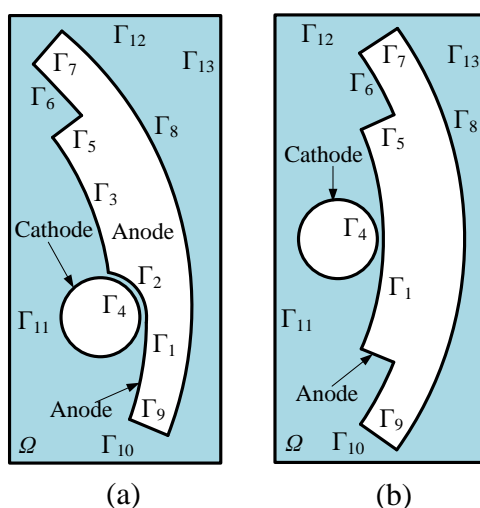


**Figure 4.** Simplified physical model of the electric potential domain: (a) single feed, (b) cyclic feed.

The contours for the current density in the machining area for single feed and cyclic feed are shown in Figure 5a and Figure 5b, respectively. Compared with the cyclic feed method, the high current density region on the anode surface of the single feed method was clearly increased. For a more intuitive comparison, the current density distributions in the processing area were processed by MATLAB and the results are shown in Figure 5c and Figure 5d. It is clear that for the single feed method, a major processing area of about 16 mm was always maintained in the high current region of more than 50 A/cm<sup>2</sup>. However, for the cyclic feed method, there was only about a 3 mm region where the current density was greater than 50 A/cm<sup>2</sup>.

To obtain a more intuitive representation of the differences in the current densities between the two methods in the main processing areas, the simulation results were substituted into Eq. 7. The results show that the total current of the single feed method reached about 106 A, while the total current for the cyclic feed method was only around 48 A. Therefore, for removal of the cast allowance, Eq. 7 would have a value greater than 1, that is to say, the single feed method would secure a greater available current than the cyclic feed method.

To better guide the experiment, the anode speed for the single feed method was evaluated

theoretically with the aid of the above simulation results. According to Eq. 1, the rotation speed of the anode can be calculated as:

$$n_a = \frac{\eta \omega i}{2\pi r} = \frac{0.00244 \times 66.3}{2 \times 3.14 \times 9} \approx 0.00286(r / \text{min}) \tag{8}$$

where  $\eta \omega$  was  $0.00258 \text{ cm}^3/(\text{A min})$ ,  $r$  was 89 mm and the current density was taken as an average value of  $68 \text{ A/cm}^2$ .

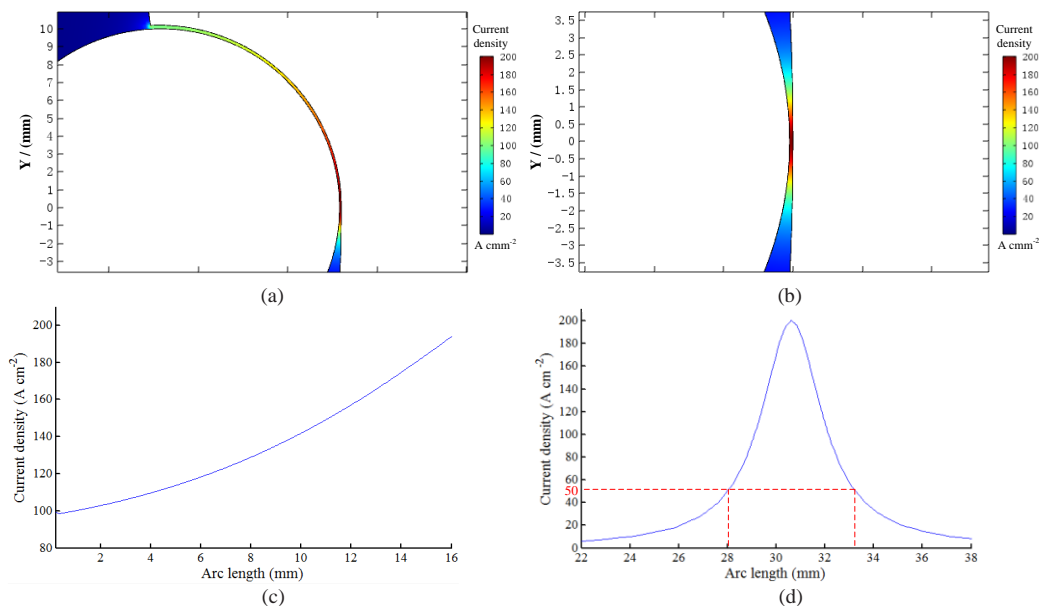


**Figure 5.** The current density distributions of the machining areas for single feed and cyclic feed operation (a) and (b) contours for current density in the machining area (c) and (d) distributions of current density for the machining areas.

### 3. EXPERIMENTAL

#### 3.1. Machining tool and experimental parameters

Experiments were conducted using a specially developed machining tool, as illustrated in Figure 6.

The anode workpiece and cathode tool were mounted on the lower and upper axes of the machine, respectively. The motions of the anode workpiece and the cathode tool, under the control of the machine tool control system, were consistent with the description given in section 2. A power generator supplied the electrical energy required in the ECM process. A real-time data acquisition module was used to collect the current signals during the machining process. A cylinder of diameter 20 mm was used as the cathode tool and the cut height was 12 mm. The machining conditions used are listed in Table 1.

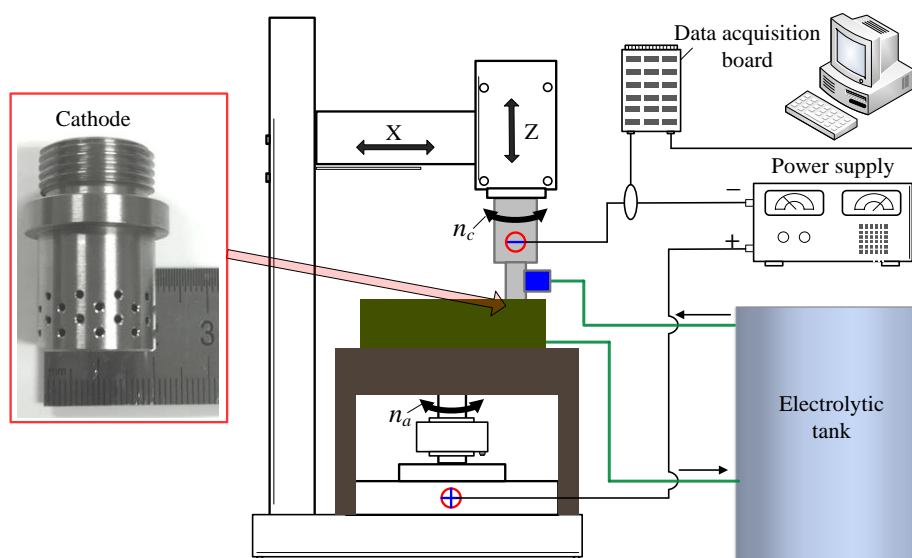


Figure 6. Schematic of the equipment and the cathode tool.

Table 1. ECM conditions

Parameter	Value
Anode workpiece	K423A
Electrolyte concentration	100g/L NaNO <sub>3</sub>
Applied voltage (V)	20
Inlet pressure (MPa)	0.2
Cathode rotation speed (rpm)	200
Initial electrode gap (mm)	0.25

### 3.2. Machining object and measurements

In the study, experiments were carried out on a simulated sample of a particular model of a cartridge receiver made of nickel-based cast superalloy K423A. Given the large size of this model of cartridge receiver, various casting risers of different shapes were used. Thus, use of a small cylindrical cathode, as proposed in this paper, as a universal cathode tool is very appropriate. In addition, some of the casting riser sizes were large, as shown in Figure 8a, with a one-sided allowance of more than 10 mm and a corresponding center angle of about 45°, so it was necessary to secure efficient processing methods.

The machining performance of the proposed methods was evaluated in terms of the material removal rate (MRR) and the machining quality. The machining quality was evaluated in terms of the angle between the ideal profile and the machined profile, as shown in Figure 7. The MRR was calculated from the following equations:

For cyclic feed operation:

$$MRR = \frac{V}{t} \tag{9}$$

where  $V$  is the removed volume and  $t$  is the machining time required to remove the cast allowance.

For single feed operation:

$$MRR = \frac{V}{\frac{b}{v} + \frac{a}{2\pi n_a}} \tag{10}$$

where  $v$  is the radial cut speed of the cathode,  $a$  is the central angle corresponding to the cast allowance shown in Figure 1 and  $n_a$  is the anode speed. Note that the feed motion in this method,  $n_a$ , needs to be precisely controlled, as described in section 2 and 3.

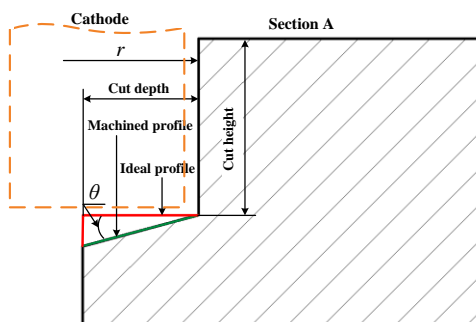


**Figure 7.** The angle between the machined profile and the ideal profile.

#### 4. RESULTS AND DISCUSSION

The casting riser structure before and after ECM is shown in Figure 8. The results indicate that both methods achieve good machining contours (see Figures 8b and 8c), thus confirming that electrolytic removal of the casting riser is viable. The angles between the machined profile and the ideal profile for the two processing methods in the A-A section are shown in Figure 9. Compared with immersion processing [19], the processing accuracy observed in this study represents a significant improvement, indicating that the present processing methods reduce the corrosion effect of stray current on the non-processing area. The angle for the single feed method was only about 2.6°, whereas the angle for the cyclic feed method was as high as 9.4°. These results indicated that the single feed method achieves better machining accuracy than the cyclic feed method.

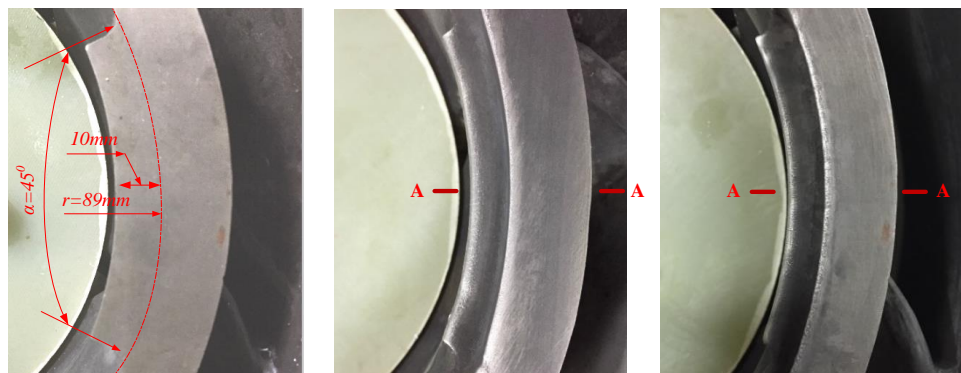


**Figure 8.** Casting riser structures: (a) before processing, (b) for the single feed method, (c) for the cyclic feed method.

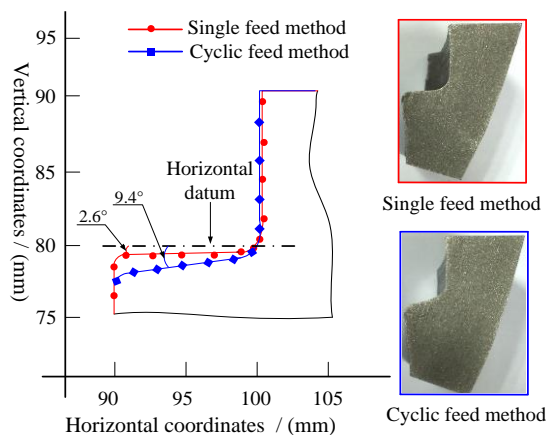


**Figure 9.** The angle between the machined profile and the ideal profile in the A-A section: (a) for the single feed method, (b) for the cyclic feed method

The current flows during ECM by the two methods were also collected and are plotted in Figure 10. It may be seen that the processing current for the single feed method (about 95 A) was much higher than the processing current (about 55 A) for the cyclic feed method, which is consistent with the simulation results for *P* in section 2, which explains why the single feed method is more efficient than the cyclic feed method. This finding is also reflected in the time course data. For the single feed method, less than 70 minutes was required to complete the processing, while the cyclic feed method required about 140 minutes. The actual anode speed for the single feed method may be calculated as follows:

$$N_a = \frac{I}{t \times 2\pi/\alpha} = \frac{I}{56 \times 8} \approx 0.00223 (rpm) \tag{11}$$

Here,  $\alpha = 45^\circ$  and  $t = 56$  (deduction of the cut-in time), and the actual anode speed was about 0.00223 rpm, which is similar to the estimated speed given by Eq. 8.

The MRR was evaluated in accordance with Eq. 9 and Eq. 10, and the results are illustrated in Figure 11. It is clear that the MRR for this study is significantly higher than that reported by Ge et al., which was about 35 mm<sup>3</sup>/min [20]. This is because the processing parameters of cut depth and cut height were larger in this work. In addition, for this study, the mass removal for the anode workpiece per unit time was as high as 928 mg/min assuming a material density of 7.98 g/cm<sup>3</sup>. This removal rate is significantly higher than that of electrochemical grinding, which is 370 mg/min [21]. This may be attributable to the higher electrochemical dissolution efficiency of the processed object [16] and the use of larger processing parameters for this study. Compared with the MRR of the single feed method, about 116.4 mm<sup>3</sup>/min, as shown in Figure 11, the MRR of the cyclic feed method was only 56.5 mm<sup>3</sup>/min. In other words, the increase in machining efficiency for the single feed method was more than two-fold. To sum up, the use of a small diameter cylinder as a universal cathode tool for efficient machining of a simulated sample by ECM is feasible, and the single feed method achieves better machining accuracy and higher machining efficiency than the cyclic feed method.

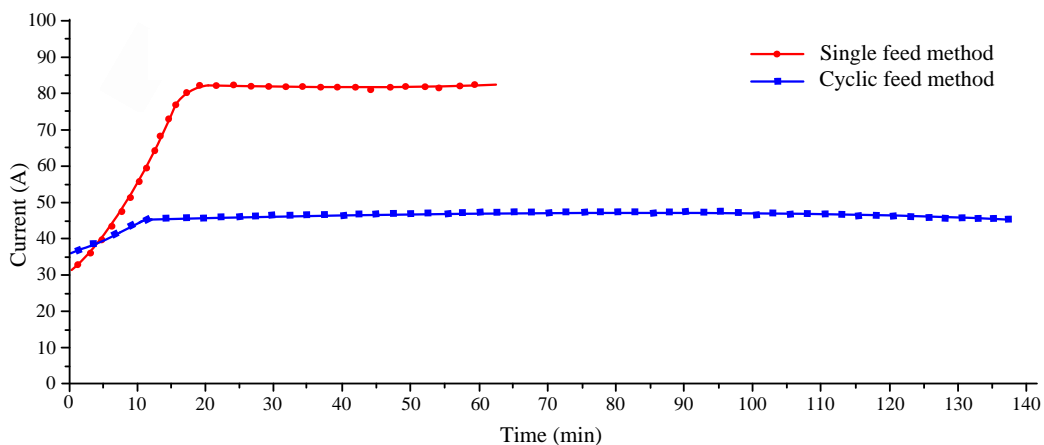


Figure 10. The current signal collected during ECM.

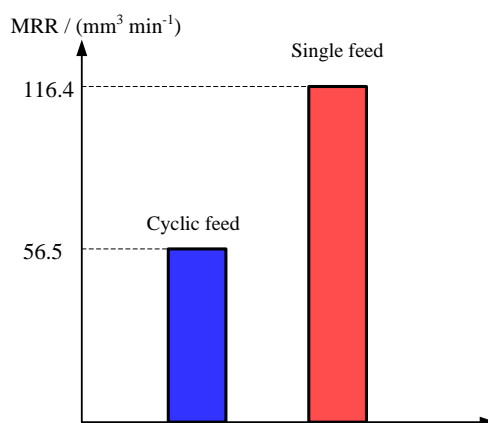


Figure 11. Comparison of MRRs for the single feed method and the cyclic feed method.

### 5. CONCLUSIONS

In this study, a small-diameter cylinder replaced the shaped cathode and was used to process a simulated sample of particular model of a cartridge receiver. Two processing methods were evaluated with the aim of achieving high-efficiency machining. Simulations and real experiments were performed. The conclusions are as follows:

- (1) A small-diameter cylinder was shown to serve as a universal cathode tool for efficient machining of a simulated sample by ECM.
- (2) The simulation results showed that the single feed method generated a larger available current than the cyclic feed method.
- (3) The experimental data showed that the single feed method achieved better machining accuracy and a higher material removal rate than the cyclic feed method.

## AUTHOR CONTRIBUTIONS

Writing of the original draft preparation, Y.G.; Investigations, Y.G., Z.Z. and W.Z.

## FUNDING

The authors wish to acknowledge the financial support provided by the State Key Program of the National Natural Science Foundation of China (51535006) and Jiangsu Key Laboratory of Precision and Micro-Manufacturing Technology.

## CONFLICTS OF INTEREST

The authors declare no conflicts of interest

## References

1. D. Lee, J. Lee, Y. Kim, J. Koo, C. Seok and Y. Kim, *Int. J. Precis. Eng. Man.*, 18 (2017) 561.
2. S. Pattnaik, D. Karunakar and P. Jha, *J. Mater. Process. Tech.*, 212 (2012) 2332.
3. T. Pollock and S. Tin, *J. Propul. Power*, 22 (2006) 361.
4. P. Caron and T. Khan, *Aerosp. Sci. Technol.*, 3 (1999) 513.
5. X.F. Chen, J.T. Li, J.T. Wu, C. Shao, S.G. Kong, W. Li, Z.Y. Pei, M. Yao and M.H. Zhao, *J. Iron Steel. Res.* 18 (2006) 51.
6. D. Szeliga, K. Kubiak, W. Ziaja and R. Cygan, *Cast Meta.*, 27 (2014) 146.
7. K. Rajurkar, D. Zhu, J. Mcgeough, J. Kozak and A. Silva, *CIRP. Ann-Manuf. Tech.*, 48 (1999) 567.
8. Z.W. Zhu, D.Y. Wang, J. Bao, N.F. Wang and D. Zhu, *Int. J. Adv. Manuf. Tech.*, 80 (2015) 1957.
9. R. Rao and V. Kalyankar, *Int. J. Adv. Manuf. Tech.* 73 (2014) 1159.
10. Y.Tang and Z.Y. Xu, *Int. J. Electrochem. Sci.* 13 (2018) 1105.
11. F. Klocke, M. Zeis, A. Klink and D. Veselovac, *Proce. Cirp.*, 6 (2013) 368.
12. Z.Y. Xu, J. Liu, D. Zhu, N.S. Qu, X.L. Wu and X.Z. Chen, *Chinese. J. Aeronaut.*, 28 (2015) 1263.
13. X.Z. Chen, Z.Y. Xu, D. Zhu, Z.D. Fang and D. Zhu, *Chinese. J. Aeronaut.*, 29 (2016) 274.
14. O. Weber, M. Weinmann, H. Natter and D. Bähre, *J. Appl. Electrochem.*, 45 (2015) 591.
15. H. Mimura and Y. Miyagawa, *J. Japan. Soc. Dent. Mater. Dev.*, 15 (1996) 283.
16. Y.C. Ge, Z.W. Zhu, D.Y. Wang, *Electrochim. Acta.*, 253 (2017) 379.
17. J.T Li, X.F. Chen, J.T. Wu, C. Shao, S.G. Kong, W. Li, Z.Y. Pei and M. Yao, *Foundry*, 55 (2006) 249.
18. D.Y. Wang, Z.Y. Zhu, H.R. Wang and D. Zhu, *Chinese. J. Aeronaut.*, 29 (2016) 534.
19. Y.C. Ge, Z.W. Zhu, M. Zhou, D.Y. Wang, *J. Electrochem. Soc.*, 165 (2018) E162.
20. Y.C. Ge, Z.W. Zhu, M. Zhou, D.Y. Wang, *J. Mater. Process. Tech.*, 258 (2018) 89.
21. H.S. Li, S. Niu, Q.L. Zhang, S.X. Fu, N.S. Qu, *Sci. Rep-UK.* 7 (2017) 3482.